Journal of Hazardous Materials 176 (2010) 139–145

Contents lists available at ScienceDirect

Journal of Hazardous Materials

journal homepage: www.elsevier.com/locate/jhazmat

Synthesis of nanocrystalline anatase TiO_2 by one-pot two-phase separated hydrolysis-solvothermal processes and its high activity for photocatalytic degradation of rhodamine B

Mingzheng Xie, Liqiang Jing*, Jia Zhou, Jingsheng Lin, Honggang Fu*

Key Laboratory of Functional Inorganic Materials Chemistry (Heilongjiang University), Ministry of Education, School of Chemistry and Materials Science, Harbin 150080, PR China

ARTICLE INFO

Article history:
Received 7 August 2009
Received in revised form 6 October 2009
Accepted 2 November 2009
Available online 10 November 2009

Keywords:
Hydrolysis-solvothermal method
Nanocrystalline TiO_2
Anatase thermal stability
Charge separation
Photocatalytic activity

ABSTRACT

Si-doped and un-doped nanocrystalline TiO_2 samples have been synthesized by simple one-pot water-organic two-phase separated hydrolysis-solvothermal (HST) processes, and characterized by XRD, BET, TEM, FT-IR, DRS and surface photovoltage techniques. The effects of the solvothermal temperature and Si doping on the anatase thermal stability, and on the photocatalytic activity for degrading rhodamine B were investigated in detail. The results show that, as the solvothermal temperature rises, the crystallinity and thermal stability of the resulting nano-sized anatase TiO_2 gradually increase. Noticeably, the as-prepared TiO_2 obtained at appropriate solvothermal temperature (160 °C) exhibits high photocatalytic activity. Moreover, although Si doping does not improve the photocatalytic activity of the as-prepared anatase TiO_2, it greatly enhances the anatase thermal stability and inhibits crystallite growth during the process of post-thermal treatment. Interestingly, the Si-doped TiO_2 post-treated at high temperature displays much higher photocatalytic activity than commercial P25 TiO_2. It is clearly demonstrated that the joint effects of high anatase crystallinity and large surface area lead to high photocatalytic activity. This work provides a simple and effective strategy for the synthesis of high-performance TiO_2-based functional nanomaterials.

1. Introduction

Semiconductor photocatalysis has attracted much attention in the past two decades owing to their applications to environmental purification [1–6]. It has been shown to be especially interesting for the treatment of dye compounds usually present in wastewaters from textile industries, because of the possibility of utilizing solar light as the energy source for the decontamination of these effluents [7–12]. Among several oxide semiconducting photocatalysts used often, TiO_2 is taken as one of the ideal photocatalysts, because of its outstanding photocatalytic activity, chemical stability, low cost and non toxicity [4–6]. It usually has two crystalline phases, anatase (Eg = 3.2 eV) and rutile (Eg = 3.0 eV), and the anatase phase frequently exhibits higher photocatalytic activity than the rutile one [6,13]. Until now, the most popular commercial TiO_2 named by Degussa P25, containing around 85% anatase and 15% rutile, usually possessed excellent photocatalytic activity [4–6]. Its high activity is mainly attributed to its mixed phase composition and high anatase crystallinity, which would favor photoinduced charge separation, as well as to large surface area (about 55 $m^2\ g^{-1}$).

In addition to the phase composition, surface area and anatase crystallinity are two important factors influencing photocatalytic performance of TiO_2. It is widely accepted that photocatalytic reactions mainly take place on the surfaces of photocatalysts. Expectedly, the adsorption of pollutants in advance is one of the most important steps in photocatalytic reactions [4–6]. Thus, large surface area is generally favorable to enhance photocatalytic activity of TiO_2. High anatase crystallinity usually means few defects, which easily act as the recombination centers for photogenerated electrons and holes [14,15]. Thus, high crystallinity would promote photocatalytic reactions. It has been demonstated that the increase in the anatase crystallinity could usually lead to the enhancement in the photocatalytic activity [16,17]. However, there is an obvious inconsistency between large surface area and high anatase crystallinity, since large surface area, often resulting from porous structure and very small particle size, usually corresponds to low anatase crystallinity of TiO_2. Therefore, the solution to the above inconsistency is the crucial to fabricate high activity TiO_2-based photocatalysts.

Thermal treatment at high temperature is generally adopted to improve anatase crystallinity of nano-sized TiO_2. However, the anatase-to-rutile transformation will happen if the treatment temperature is too high (over 600 °C). On the basis of the phase transformation mechanism that the rutile phase starts to occur at

* Corresponding authors. Tel.: +86 451 86608616; fax: +86 451 86673647.
E-mail addresses: Jinglq@hlju.edu.cn (L. Jing), Fuhg@vip.sina.com (H. Fu).

0304-3894/$ – see front matter © 2009 Published by Elsevier B.V.
doi:10.1016/j.jhazmat.2009.11.008

the interfaces between the anatase particles in the agglomerated TiO_2 particles [18], it is expected that the phase transformation usually leads to the remarkable increase in the particle size and consequently make surface area greatly decrease. Therefore, it is predicted that the increase in the anatase thermal stability might be a feasible strategy to solve the inconsistent issue mentioned above.

The sol–gel technique based on the hydrolysis of titanium alkoxide is widely developed to synthesize nano-sized TiO_2 [19]. However, this technique usually has marked shortcomings, such as weak anatase crystallinity, complicated synthesis and post-treatment procedures, poor monodispersity, and possibly accompanied by too much of waste liquids. Those shortcomings would greatly influence the performance and large-scale production and successful applications in industry of the resulting TiO_2 nanomaterials. Thus, simple methods that are easily operated to obtain monodispersed nanocrystalline TiO_2 simultaneously with high anatase crystallinity are still desired. Very recently, Tang et al. developed a one-step synthesis method to prepare high-quality ultrafine inorganic semiconductor nanocrystals via a two-phase interface hydrolysis reaction under hydrothermal conditions [20], which is named by the two-phase separated hydrolysis-solvothermal (HST) process in our work, and mainly demonstrated that the prepared ZrO_2 nanocrystals have good monodispersity and high crystallinity. This newly developed method spurs us to carry out this work, in which we aim to design and synthesize high active nano-sized TiO_2-based photocatalysts.

Herein, we synthesize Si-doped and un-doped nanocrystalline TiO_2 by the simple one-pot phase separated HST processes. It is found that the un-doped TiO_2 obtained at 160 °C exhibits higher photocatalytic activity than that prepared by the traditional sol-hydrothermal method at the same temperature. Moreover, the resulting Si-doped TiO_2 post-treated at high temperature exhibits much higher photocatalytic activity than well-known P25 TiO_2. These findings are in good agreement with our expectations. It should be suggested that the joint effects of high anatase crystallinity and large surface area are responsible for the high photocatalytic activity. This work would provide an effective strategy to design and fabricate high-performance TiO_2-based functional materials with high anatase thermal stability, and further expand the application areas due to high anatase thermal stability.

2. Experimental section

All used chemicals are of the analytical grade and are used as received without further purification, and doubly deionized water is employed throughout.

2.1. Synthesis of materials

Nano-sized TiO_2 is synthesized by the HST process [20]. The key point to the synthetic reaction is to combine the hydrolysis and nucleation process at the confined water/toluene interface with the subsequent crystallization process in the toluene under solvothermal condition. A 30 mL of Teflon lined stainless-steel vessel, in which a 10 mL of weight bottle is installed to contain the organic toluene, is used as the reaction device to carry out the HST experiment. In a typical process, 10 mL of water phase and 8 mL of toluene phase, which contains a desired amount of $Ti(OBu)_4$, was placed in the device separately. Then, the sealed device is kept at certain temperature (120–200 °C) for 2 h, followed by naturally cooling to room temperature. Under the solvothermal conditions, both the water and toluene are evaporated to diffuse gradually to the other side to form an interface. It is expected that the interface may locate near the organic phase side since the toluene has a higher boiling point than the water. When the water steam and toluene steam containing a certain amount of $Ti(OBu)_4$ molecules meet, the hydrolysis reaction between $Ti(OBu)_4$ and water will occur immediately, simultaneously leading to the crystal nucleus of TiO_2. Then, the formed crystal nucleus is further crystallized in the organic phase. Thus, the resulting nanocrystalline TiO_2 is collected in the toluene, and subsequently the dried TiO_2 nanopowder is obtained by distilling the toluene system at 120 °C. At last, different TiO_2 samples are produced by further calcining dried TiO_2 at different temperature for 2 h. T*X*-*Y*, in which *X* is the solvothermal temperature and *Y* is the calcination temperature, is used to represent the specific TiO_2 sample. In addition, to obtain Si-doped TiO_2 by the HST process, a desired amount of $(C_2H_4O)_4Si$ and $Ti(OBu)_4$ are added together to the organic phase, and ST*X*-*Y* indicates the 3 in mole % Si-doped TiO_2 sample.

2.2. Characterization of materials

The samples are characterized by X-ray powder diffraction (XRD) with a Rigaku D/MAX-rA powder diffractometer (Japan), using Cu Kα radiation (λ = 0.15418 nm), and an accelerating voltage of 30 kV and emission current of 20 mA are employed; The specific surface areas of the samples are measured by BET instrument (Micromeritics automatic surface area analyzer Gemini 2360, Shimadzu), with nitrogen adsorption at 77 K; Transmission electron microscopy (TEM) observation was completed on a JEOL JEM-2010EX instrument operated at 200 kV accelerating voltage; The Fourier transform infrared spectra (FT-IR) of the samples are collected with a Bruker Equinox 55 Spectrometer, using KBr as diluents; The ultraviolet–visible diffuse reflectance spectra (UV–vis DRS) of the samples are recorded with a Model Shimadzu UV2550 spectrophotometer; The SPS measurements of the samples are carried out with a home-built apparatus that had been described in detail elsewhere [21–23].

2.3. Evaluation of photocatalytic activity

Rhodamine B (RhB) is commonly used as a dye, and it has been found to be potentially toxic and carcinogenic [24]. Thus, RhB is chosen as the representative organic dye pollutant to evaluate photocatalytic activity of the as-prepared TiO_2. Photocatalytic experiments are carried out in a 100 mL of photochemical glass reactor, and the similar solar light is provided from a side of the reactor by a 150 W GYZ220 high-pressure Xenon lamp made in china without any filter, which is placed at about 10 cm from the reactor. During the measurements of photocatalytic degradation rate of RhB, 0.05 g of the TiO_2 sample and 60 mL of 50 mg/L RhB solution are mixed by a magnetic stirrer for 30 min in the dark first, in order to make the reactive system uniform and the adsorption equilibrium, then begin to illuminate. After photocatalytic reaction for 1 h, the RhB concentration is analyzed by means of the optical characteristic absorption at 553 nm after centrifugation with a Model Shimadzu UV2550 spectrophotometer [24]. To obtain the evolution curves of photocatalytic degradation of RhB, 0.1 g of the TiO_2 sample and 60 mL of 50 mg/L RhB (15 mg/L phenol) solution are employed and the RhB concentrations after photocatalytic reaction for different time are measured.

3. Results and discussion

3.1. Measurements of XRD and BET

The XRD peaks at $2\theta = 25.28°$ and $2\theta = 27.40°$ are often taken as the characteristic peaks of anatase (1 0 1) and rutile (1 1 0) crystal phase, respectively [25,26]. The mass percentage of anatase phase in the TiO_2 samples can be estimated from the respective integrated characteristic XRD peak intensities using the quality factor

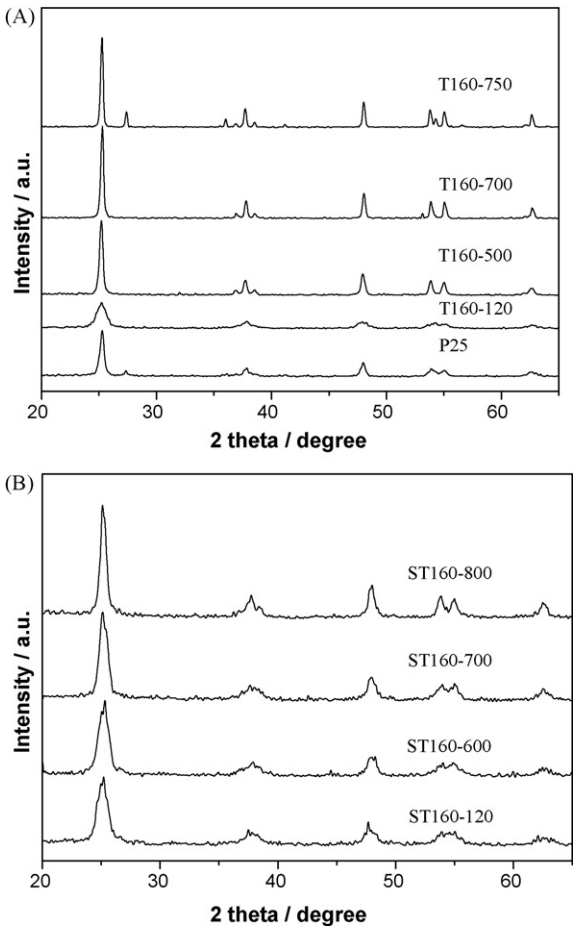

Fig. 1. XRD patterns of different TiO_2 samples.

ratio of anatase-to-rutile (1.265), and the crystallite size can also be determined from the broadening of corresponding X-ray spectral peak by Scherrer formula [26]. Fig. 1 shows the XRD patterns of different TiO_2 samples, including home-made un-doped and Si-doped TiO_2 and commercial P25 TiO_2. It is seen from the Fig. 1 that the T160-120 sample has a pure anatase phase, and its crystallite size is 6.6 nm. As the thermal treatment temperature increases, the anatase XRD peaks gradually become strong, indicating that the anatase crystallinity increases, meanwhile the corresponding crystallite size gradually becomes large (Table 1). When the temperature increases to 750 °C, however, the rutile phase (17%) appears, indicating that the phase transformation begins to take place. In general, the beginning temperature of phase transformation of nano-sized anatase TiO_2 prepared by the sol process is generally at about 600 °C [5,14]. It should be pointed that the T160-120 sample exhibits high anatase crystallinity and large crystallite size compared with that obtained by the sol-hydrothermal process at the same temperature based on the XRD patterns, shown in the supporting information (SI-I). High anatase crystallinity and large crystallite size mean low surface energy, and the low surface energy is unfavorable to the phase transformation process, consequently leading to the enhancement in the beginning phase transformation temperature. This is also further supported by the results that the XRD intensity of the resulting TiO_2 gradually increases and the corresponding beginning phase transformation temperature also rises as the solvothermal temperature is enhanced supporting information (SI-I). Moreover, it is expected that the high dispersity of the original anatase nanocrystals obtained by the HST process, which had been well demonstrated [20], also should play an important role in the inhibition phase transformation process based on the mechanism mentioned above [18]. Therefore, it can be deduced that the enhanced beginning phase transformation temperature is attributed to the high crystallinity, large crystallite size and high dispersity of the as-prepared anatase crystallites.

Table 1
Phase composition, crystallite size and surface area of different TiO_2 samples.

Sample	Phase composition (%)		Crystallite size (nm)	Surface area ($m^2\,g^{-1}$)
	Anatase	Rutile		
T160-120	100	–	6.6	131.9
T160-500	100	–	20.7	56.4
T160-700	100	–	25.3	41.6
T160-750	83	17	28.1	26.2
ST160-120	100	–	7.4	152.3
ST160-600	100	–	8.1	128.9
ST160-700	100	–	9.4	89.5
ST160-800	100	–	11.5	63.4
P25	82	18	19.5	58.2

As the thermal treatment temperature increases, the anatase XRD peaks of the Si-doped TiO_2 gradually increase, demonstrating that the corresponding anatase crystallinity becomes high. Interestingly, compared with the un-doped TiO_2, the Si-doped TiO_2 exhibits high anatase thermal stability since no rutile appears in the Si-doped TiO_2 by the thermal treatment at 800 °C. This demonstrates that the introduction of Si inhibits the phase change, which is in good agreement with the literatures [27,28]. In addition, the phases related to Si are not detected from XRD patterns.

For the un-doped TiO_2, the T160-120 has a large BET surface area ($131.9\,m^2\,g^{-1}$) (Table 1), and the surface area obviously decreases as the thermal treatment temperature increases. Noticeably, Si doping effectively maintains the large surface area of nano-sized TiO_2. After thermal treatment at the temperature as high as 800 °C, the ST800 still has larger surface area than P25 TiO_2.

3.2. Measurements of TEM and FT-IR

The TEM photographs of different TiO_2 samples are shown in Fig. 2. It can be seen that all the samples have similar spherical form. The T160-120 has an about 7 nm average particle size with narrow size distribution (Fig. 2A), which is in accordance with the crystallite size evaluated by the Scherrer formula, indicating that the obtained TiO_2 crystallites are easily separated. After the thermal treatment at 750 °C, the average particle size of the un-doped TiO_2 has increased to about 30 nm, with wide size distribution (Fig. 2B), which is attributed to the occurrence of rutile based on the XRD patterns, accompanied by the particle agglomeration [18]. By comparison, it can be noticed that Si doping effectively inhibits the growth of nanocrystalline TiO_2, since the ST160-120 and ST160-800 exhibit about 6.0 and 12 nm particle sizes, respectively, both with narrow size distribution (Fig. 2C and D). Thus, these TEM observations are well responsible for the corresponding surface areas listed in the Table 1.

Fig. 3 shows the FT-IR spectra of different TiO_2 samples. The IR peaks at about 1630 and 3400 cm^{-1} are ascribed to surface hydroxyl and adsorbed water molecules [29,30]. The IR band at 400–850 cm^{-1} corresponds to the Ti–O–Ti stretching vibration mode in crystal TiO_2 [29]. The IR peaks at about 3000 and 1497 cm^{-1} are ascribed to the C–H and C=C stretching vibration mode in aromatic ring [31].

As the thermal treatment temperature increases, the intensity of IR band related to Ti–O–Ti vibration mode also increases, indicating that the corresponding TiO_2 crystallinity becomes high, which is in accordance with the XRD results. Moreover, the surface hydroxyl amount of the Si-doped TiO_2 sample gradually decreases. However, the ST160-800 still displays a larger amount of surface hydroxyl

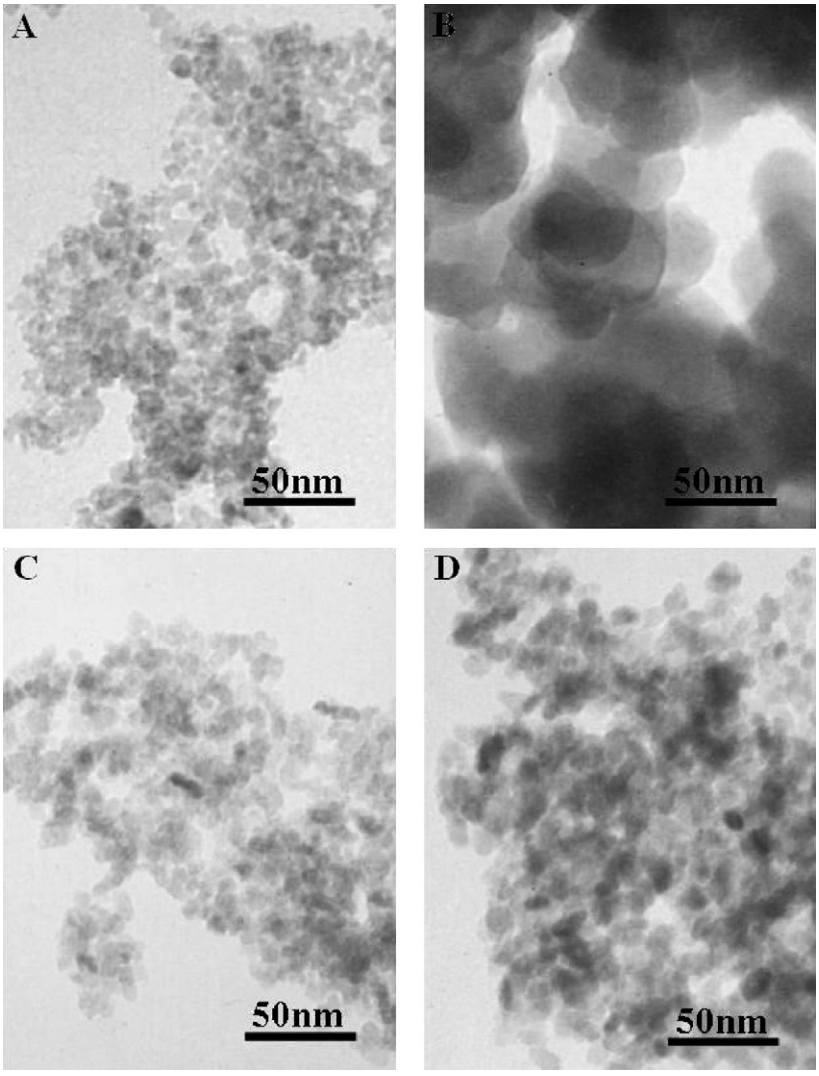

Fig. 2. TEM images of different TiO_2 samples (A) T160-120, (B) T160-750, (C) ST160-120, (D) ST160-800.

than the T160-700. In addition, all the Si-doped TiO_2 samples have a IR peak at about 1050 cm^{-1}, which results from Si–O–Si mode in SiO_2 [32].

Based on the above analyses of XRD, TEM and IR, it can be deduced that Si doping inhibits the anatase-to-rutile phase transformation and simultaneous particle growth of nanocrystalline TiO_2, which is attributed to the existence of amorphous SiO_2. The SiO_2 would hold back the contacts between the anatase nanocrystals, the diffusions between anatase crystallites, and the surface ionic mobilities [27,32–35].

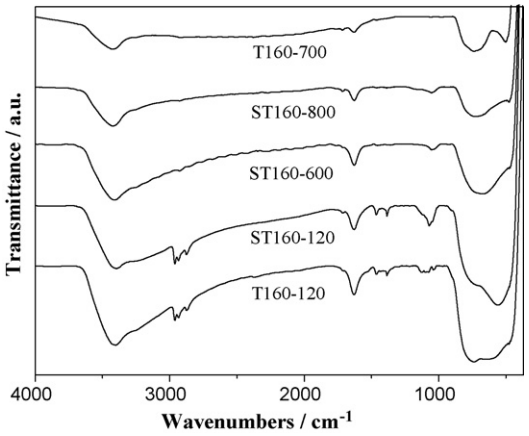

Fig. 3. IR spectra of different TiO_2 samples.

3.3. Measurements of DRS and SPS

The UV–vis DRS spectra of different TiO_2 are shown in Fig. 4. According to the energy band structure of TiO_2, it can be confirmed that the strong optical absorption below 390 nm is mainly attributed to the electron transitions from the valence band to conduction band [21,29]. It can be noticed that the DRS spectrum of the doped TiO_2 shifts slightly to the red with increasing the treatment temperature from 120 to 800 °C, which strongly demonstrates that the crystallite size and the phase transformation are effectively suppressed. This is in good agreement with the above XRD and TEM results.

The surface photovoltage generation mainly arises from the creation of electron-hole pairs, followed by the separation under a built-in electric field, also called space-charge layer. Thus, it can be expected that the stronger is the surface photovoltage spectroscopy (SPS) response, the higher is the photoinduced charge carrier [36,21]. Fig. 5 shows the SPS responses of different TiO_2 sam-

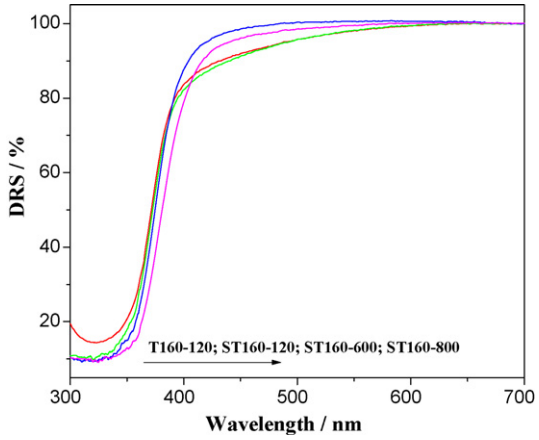

Fig. 4. DRS spectra of different TiO_2 samples.

ples. For all the samples, an obvious SPS response can be found at the wavelength range from 300 to 375 nm, which is attributed to the electron transitions from the valence band to conduction band ($O_{2p} \rightarrow Ti_{3d}$) on the basis of the DRS spectra and TiO_2 band structure [21,29]. For the Si-doped TiO_2 sample with anatase phase composition, the SPS response gradually becomes strong with increasing the treatment temperature, which is mainly because of the increase in the antatase crystallinity. The high crystallinity makes electronic band perfect so as to enhance the built-in field strength, which can promote charge separation [22], meanwhile leads to the decrease in the defect amounts, which is also favorable for charge separation [37,14]. This is also supported by the point that the SPS response of un-doped TiO_2 increases as the solvothermal temperature or the post-treatment temperature is enhanced supporting information (SI-II). However, compared with the un-doped TiO_2, all the Si-doped TiO_2 samples exhibit low SPS responses, which are possibly ascribed to the SiO_2 as the nonconductor. In addition to the band-to-band SPS response, a weak SPS response related to surface states, located at the wavelength range from 375 to 420 nm, is found in the ST160-800 sample. This surface state-related SPS response might result from the electronic transitions from the anatase surface states to the rutile conduction band in the phase-mixed TiO_2 [38]. According to the above XRD results, there is not rutile phase in the ST800. Actually, there might be a small amount of rutile since the XRD detection is very limited.

3.4. Photocatalytic activity

Generally speaking, the high photocatalytic degradation rate corresponds to the high photocatalytic activity. In the photocatalytic experiment, The 150 W Xenon lamp, with similar emitting spectrum to the sun, is used as light resource. Compared with the photocatalytic degradation, the direct photolysis (1%) is so small that the corresponding degradation is neglectable. The photocatalytic degradation rates of RhB, which equal to the differences between the total degradation rates in the presence of light and the adsorption degradation rates in the absence of light, on the different TiO_2 samples, are shown in the Fig. 6.

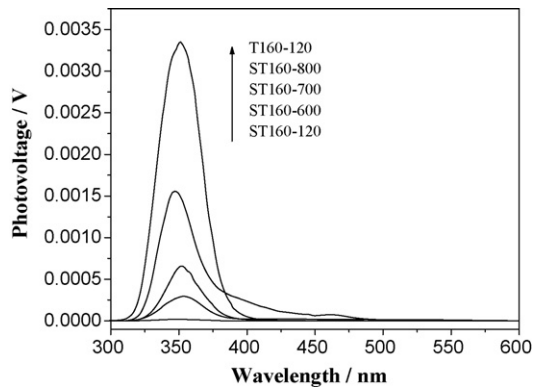

Fig. 5. SPS responses of different TiO_2 samples.

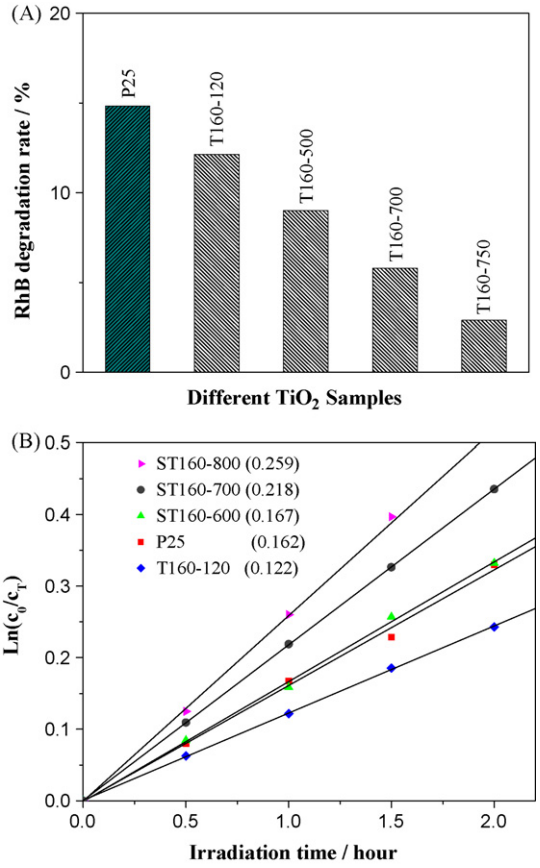

Fig. 6. Photocatalytic degradation rates (A) and evolution curves (B) of RhB solution on different TiO_2 samples (the corresponding degradation rate constants are listed in the parentheses).

It can be seen from Fig. 6A that, for the un-doped TiO_2, the photocatalytic activity gradually decreases as the thermal treatment temperature increases. This seems un-imaginable since the photoinduced charge separation situation should be improved with increasing the treatment temperature on the basis of SPS responses supporting information (SI-II). Thus, it is deduced that the decrease in the activity is mainly attributed to the great decrease in the surface area shown in Table 1. However, it should be pointed that, among the as-prepared three TiO_2 samples at the solvothermal temperatures of 120, 160 and 200 °C, the TiO_2 obtained at 160 °C displays the highest activity, and also it is superior to the TiO_2 obtained by the traditional sol-hydrothermal process at the same temperature supporting information (SI-III). It is expected that the high activity of the T160-120 is attributed to the high anatase crystallinity and the high crystallite monodispersity [20].

As expected, it can be confirmed from the photocatalytic degradation rates of RhB (Fig. 6B) that the Si-doped TiO_2 gradually exhibits much high photocatalytic activity as the thermal treatment temperature is enhanced. Noticeably, the TiO_2 sample by thermal treatment over 600 °C possesses high activity compared with the P25 TiO_2, which is also proved by the photocatalytic degradation of phenol Appendix B(SI-III). Based on the above SPS, TEM

and BET measurements, it is concluded that the high photoindued charge separation rate, small particle size and large surface area are responsible for the high photocatalytic activity of Si-doped TiO_2 treated at high temperature. Moreover, a certain amount of surface hydroxyl and rutile phase are also favorable for photocatalytic reactions [17]. In addition, it is also confirmed that the RhB photocatalytic degradation processes in our experiments follow one-order reactions, which is accordance with the literature [39].

4. Conclusions

On the basis of the above systematic investigation, mainly by means of XRD, BET, TEM, IR and SPS measurements, the following conclusions can be drawn: (i) Nanocrystalline TiO_2 with high anatase crystallinity and high crystallite monodispersity is successfully synthesized by the HST processes, and its anatase thermal stability is enhanced with increasing the solvothermal temperature. (ii) The as-prepared nanocrystalline TiO_2 obtained at 160 °C exhibits higher photocatalytic activity than that prepared by the transitional sol-thermal method at the same hydrothermal temperature, demonstrating that the HST route is an extremely effective synthetic approach. (iii) As expected, Si doping greatly enhances the anatase thermal stability, meanwhile effectively inhibiting the growth of the TiO_2 crystallites, resulting in high photocatalytic activity, superior to that of P25 TiO_2.

It is suggested that the photocatalytic activity of nano-sized TiO_2 is jointly determined by the photoinduced charge separation ability and the surface area. Based on the SPS responses, high anatase crystallinity, which can be produced by enhancing the anatase thermal stability, greatly favors photoinduced charge separation. The phase separated SHT synthesis overcomes the difficulty of producing high anatase crystallinity and also with large surface area, resulting in highly active nanostructured TiO_2-based functional materials with high thermal stability.

Acknowledgements

This work is financially supported from the National Nature Science Foundation of China (No. 20501007), the programme for New Century Excellent Talents in universities (NCET-07-0259), the Key Project of Science & Technology Research of Ministry of Education of China (No. 207027) and the Science Foundation of Excellent Youth of Heilongjiang Province of China (JC200701), for which we are very grateful.

Appendix A. Supplementary data

Supplementary data associated with this article can be found, in the online version, at doi:10.1016/j.jhazmat.2009.11.008.

References

[1] O. Legrini, E. Oliveros, M.M. Braun, Photochemical processes for water treatment, Chem. Res. 93 (1993) 671–698.
[2] M.A. Fox, M.T. Dulay, Heterogeneous photocatalysis, Chem. Res. 93 (1993) 341–357.
[3] J. Kirchnerova, M.L. Herrera Cohen, C. Guy, D. Klvana, Photocatalytic oxidation of *n*-butanol under fluorescent visible light lamp over commercial TiO_2 (Hombicat UV100 and Degussa P25), Appl. Catal. A 282 (2005) 321–332.
[4] P.V. Kamat, Photochemistry on nonreactive and reactive (semiconductor) surfaces, Chem. Res. 93 (1993) 267–300.
[5] M.R. Hoffmann, S.T. Martin, W. Choi, D.W. Bahnemann, Environmental applications of semiconductor photocatalysis, Chem. Res. 95 (1995) 69–96.
[6] M.I. Litter, Heterogeneous photocatalysis: transition metal ions in photocatalytic systems, Appl. Catal. B 23 (1999) 89–114.
[7] H. Lachheb, E. Puzenat, A. Houas, M. Ksibi, E. Elaloui, C. Guillard, J.-M. Herrmann, Photocatalytic degradation of various types of dyes (Alizarin S, Crocein Orange G, Methyl Red, Congo Red, Methylene Blue) in water by UV-irradiated titania, Appl. Catal. B 39 (2002) 75–90.
[8] I.K. Konstantinou, T.A. Albanis, TiO_2-assisted photocatalytic degradation of azo dyes in aqueous solution: kinetic and mechanistic investigations: a review, Appl. Catal. B 49 (2004) 1–14.
[9] E. Bizani, K. Fytianos, I. Poulios, V.J. Tsiridis, Photocatalytic decolorization and degradation of dye solutions and wastewaters in the presence of titanium dioxide, Hazard. Mater. 136 (2006) 85–94.
[10] V. Augugliaro, C. Baiocchi, A. Bianco Prevot, E. Garciá-Lopéz, V. Loddo, S. Malato, G. Marcı ĭ, L. Palmisano, M. Pazzi, E. Pramauro, Azo dyes photocatalytic degradation in aqueous suspension of TiO_2 under solar irradiation, Chemosphere 49 (2002) 1223–1230.
[11] M. Stylidi, D.I. Kondarides, X.E. Verykios, Pathways of solar light-induced photocatalytic degradation of azo dyes in aqueous TiO_2 suspensions, Appl. Catal. B 40 (2003) 271–286.
[12] D. Zhao, C.C. Chen, Y.F. Wang, H.W. Ji, W.H. Ma, L. Zang, J.C. Zhao, Surface modification of TiO_2 by phosphate: effect on photocatalytic activity and mechanism implication, J. Phys. Chem. C 112 (2008) 5993–6001.
[13] W. Li, C. Liu, Y. Zhou, Y. Bai, X. Feng, Z.H. Yang, L.H. Lu, X.H. Lu, K.Y. Chan, Enhanced photocatalytic activity in anatase/TiO_2(B) core-shell nanofiber, J. Phys. Chem. C 112 (2008) 20539–20545.
[14] G.H. Tian, H.G. Fu, L.Q. Jing, B.F. Xin, K. Pan, Preparation and characterization of stable biphase TiO_2 photocatalyst with high crystallinity, large surface area, and enhanced photoactivity, J. Phys. Chem. C 112 (2008) 3083–3089.
[15] S.C. Pillai, P. Periyat, H. George, D.E. McCormack, M.K. Seery, H. Hayden, J. Colreavy, D. Corr, S.J. Hinder, Synthesis of high temperature stable anatase TiO_2 photocatalyst, J. Phys. Chem. C 111 (2007) 1605–1611.
[16] B. Ohtani, S. Nishimoto, Effect of surface adsorptions of aliphatic alcohols and silver ion on the photocatalytic activity of titania suspended in aqueous solutions, J. Phys. Chem. 97 (1993) 920–926.
[17] C.H. Kang, L.Q. Jing, T. Guo, H.C. Cui, J. Zhou, H.G. Fu, Mesoporous SiO_2-modified nanocrystalline TiO_2 with high anatase thermal stability and large surface area as efficient photocatalyst, J. Phys. Chem. C 113 (2009) 1006–1013.
[18] J. Zhang, M.J. Li, Z.C. Feng, J. Chen, C. Li, UV Raman spectroscopic study on TiO_2. I. Phase transformation at the surface and in the bulk, J. Phys. Chem. B 110 (2006) 927–935.
[19] B.B. Lakshmi, C.J. Patrissi, C.R. Martin, Sol–gel template synthesis of semiconductor oxide micro- and nanostructures, Chem. Mater. 9 (1997) 2544–2550.
[20] K.J. Tang, J.N. Zhang, W.F. Yan, Z.H. Li, Y.D. Wang, W.M. Yang, Z.K. Xie, T.L. Sun, Harald Fuchs, One-step controllable synthesis for high-quality ultrafine metal oxide semiconductor nanocrystals via a separated two-phase hydrolysis reaction, J. Am. Chem. Soc. 130 (2008) 2676–2680.
[21] L.Q. Jing, Z.L. Xu, J. Shang, X.J. Sun, W.M. Cai, H.G. Fu, Review of surface photovoltage spectra of nano-sized semiconductor and its applications in heterogeneous photocatalysis, Sol. Energy Mater. Sol. C. 79 (2003) 133–151.
[22] Y.H. Lin, D.J. Wang, Q.D. Zhao, M. Yang, Q.L. Zhang, A study of quantum confinement properties of photogenerated charges in ZnO nanoparticles by surface photovoltage spectroscopy, J. Phys. Chem. B 108 (2004) 3202–3207.
[23] B.F. Xin, L.Q. Jing, Z.Y. Ren, B.Q. Wang, H.G. Fu, Effects of simultaneously doped and deposited Ag on the photocatalytic activity and surface states of TiO_2, J. Phys. Chem. B 109 (2005) 2805–2809.
[24] J.C. Zhao, T.X. Wu, K.Q. Wu, K. Oikawa, H. Hidaka, N. Serpone, Photoassisted degradation of dye pollutants. 3. Degradation of the cationic dye rhodamine B in aqueous anionic surfactant/TiO_2 dispersions under visible light irradiation: evidence for the need of substrate adsorption on TiO_2 particles, Environ. Sci. Technol. 32 (1998) 2394–2400.
[25] L.Q. Jing, B.F. Xin, F.L. Yuan, L.P. Xue, B.Q. Wang, H.G. Fu, Effects of surface oxygen vacancies on photophysical and photochemical processes of Zn-doped TiO_2 nanoparticles and their relationships, J. Phys. Chem. B 110 (2006) 17860–17865.
[26] Q.H. Zhang, L. Gao, J.K. Guo, Effects of calcination on the photocatalytic properties of nano-sized TiO_2 powders prepared by $TiCl_4$ hydrolysis, Appl. Catal. B 26 (2000) 207–215.
[27] M. Hirano, K. Ota, H. Iwata, Direct formation of anatase (TiO_2)/silica (SiO_2) composite nanoparticles with high phase stability of 1300 °C from acidic solution by hydrolysis under hydrothermal condition, Chem. Mater. 16 (2004) 3725–3732.
[28] G. Calleja, D.P. Serrano, R. Sanz, P. Pizarro, Mesostructured SiO_2-doped TiO_2 with enhanced thermal stability prepared by a soft-templating sol–gel route, Microporous Mesoporous Mater. 111 (2008) 429–440.
[29] L.Q. Jing, H.G. Fu, B.Q. Wang, D.J. Wang, B.F. Xin, S.D. Li, J.Z. Sun, Effects of Sn dopant on the photoinduced charge property and photocatalytic activity of TiO_2 nanoparticles, Appl. Catal. B 62 (2006) 282–291.
[30] Z. Ding, G.Q. Lu, P.F. Greenfield, Role of the crystallite phase of TiO_2 in heterogeneous photocatalysis for phenol oxidation in water, J. Phys. Chem. B 104 (2000) 4815–4820.
[31] T.A. Gordymova, A.A. Budneva, A.A. Davydov, IR spectra of toluene adsorbed on γ-Al_2O_3, React. Kinet. Catal. Lett. 20 (1982) 113–117.
[32] K.Y. Jung, S.B. Park, Enhanced photoactivity of silica-embedded titania particles prepared by sol–gel process for the decomposition of trichloroethylene, Appl. Catal. B 25 (2000) 249–256.
[33] W. Dong, Y. Sun, C.W. Lee, W. Hua, X. Lu, Y. Shi, S. Zhang, J. Chen, D. Zhao, Controllable and repeatable synthesis of thermally stable anatase nanocrystal-silica composites with highly ordered hexagonal mesostructures, J. Am. Chem. Soc. 129 (2007) 13894–13904.
[34] J.C. Yu, L. Zhang, Z. Zheng, J. Zhao, Synthesis and characterization of phosphated mesoporous titanium dioxide with high photocatalytic activity, Chem. Mater. 15 (2003) 2280–2286.

[35] Q.F. Li, W. Yuan, D.S. Ai, C.S. Deng, X.M. Dai, Photocatalytic properties of TiO_2 and Fe(III)-, Zn(II)-and Si(IV)-doped TiO_2 nanopowders synthesized by sol–gel, Ceram. Trans. 193 (2006) 165–173.
[36] L. Kronik, Y. Shapira, Surface photovoltage phenomena: theory, experiment, and applications, Surf. Sci. Rep. 37 (1999) 1–206.
[37] D. He, F. Lin, Preparation and photocatalytic activity of anatase TiO_2 nanocrystallites with high thermal stability, Mater. Lett. 61 (2007) 3385–3387.
[38] L.Q. Jing, S.D. Li, S. Song, L.P. Xue, H.G. Fu, Investigation on the electron transfer between anatase and rutile in nano-sized TiO_2 by means of surface photovoltage technique and its effects on the photocatalytic activity, Sol. Energy Mater. Sol. C. 92 (2008) 1030–1036.
[39] M. Asiltürk, F. Sayılkan, S. Erdemoğlu, M. Akarsu, H. Sayılkan, M. Erdemoğlu, E. Arpac, Characterization of the hydrothermally synthesized nano-TiO_2 crystallite and the photocatalytic degradation of rhodamine B, J. Hazard Mater. 129 (2006) 164–170.